

Discovering true muonium at LHCb

Xabier Cid Vidal,^{1,*} Philip Ilten,^{2,†} Jonathan Plews,^{2,‡} Brian Shuve,^{3,4,§} and Yotam Soreq^{5,6,||}

¹*Instituto Galego de Física de Altas Enerxías (IGFAE), Universidade de Santiago de Compostela, 15782 Santiago de Compostela, Spain*

²*School of Physics and Astronomy, University of Birmingham, Birmingham B152 2TT, United Kingdom*

³*Harvey Mudd College, 301 Platt Boulevard, Claremont, California 91711, USA*

⁴*University of California, 900 University Avenue, Riverside, California 92521, USA*

⁵*Theoretical Physics Department, CERN, CH-1211 Geneva 23, Switzerland*

⁶*Department of Physics, Technion, Haifa 32000, Israel*



(Received 3 May 2019; published 10 September 2019)

We study the potential of the LHCb experiment to discover, for the first time, the $\mu^+\mu^-$ true muonium bound state. We propose a search for the vector 1^3S_1 state, \mathcal{TM} , which kinetically mixes with the photon and dominantly decays to e^+e^- . We demonstrate that a search for $\eta \rightarrow \gamma\mathcal{TM}$, $\mathcal{TM} \rightarrow e^+e^-$ in a displaced vertex can exceed a significance of 5 standard deviations assuming statistical uncertainties. We present two possible searches: an inclusive search for the e^+e^- vertex, and an exclusive search which requires an additional photon and a reconstruction of the η mass.

DOI: [10.1103/PhysRevD.100.053003](https://doi.org/10.1103/PhysRevD.100.053003)

I. INTRODUCTION

Electromagnetic (EM) interactions between oppositely charged particles form bound states; by far, the most well known of these are the atoms. Similar atomlike bound states of elementary particles have since been discovered, including positronium (a bound state of e^+e^-) [1] and muonium (a bound state of μ^+e^-) [2]. The properties of these bound states are predicted by quantum electrodynamics (QED), and measurements of the mass and spectra provide precision tests of QED.

However, there remain heavier QED bound states that have not yet been experimentally observed which can provide unique probes that are sensitive to beyond the standard model (BSM) physics. In particular, the hypothesized bound state known as true muonium ($\mu^+\mu^-$) [3] has yet to be discovered. In this work, we explore the potential of the LHCb experiment to discover the lowest spin-1 state of true muonium via its displaced decays to e^+e^- pairs. We show that true muonium can be observed with a statistical significance exceeding 5 standard deviations using the

expected 15 fb^{-1} of LHC Run 3 data to be collected with the upgraded LHCb detector [4–9].

The most promising true muonium state for discovery is the 1^3S_1 state, which in the nonrelativistic limit has zero orbital angular momentum and is in the spin-triplet state. This vector muonium state, which we denote as \mathcal{TM} , kinetically mixes with the photon resulting in a phenomenology similar to the dark photon [10–15]. Dark photons have been the subject of much recent study, e.g., [16–18], allowing us to use these latest developments in the discovery of \mathcal{TM} at LHCb. Note that spin-singlet true muonium states also exist, but their dominant decay are to $\gamma\gamma$, which is challenging to reconstruct with the LHCb detector. Therefore, we concentrate on the discovery of \mathcal{TM} , the spin-triplet true muonium state.

Other possible search avenues for \mathcal{TM} are with the currently running HPS experiment [19] or via rare B decays into leptonium at LHCb [20]. However, both of these methods are statistically limited with potentially large backgrounds and are not expected to have discovery potential. The proposed RedTop [21,22] experiment at Fermilab is designed to produce a large flux of η mesons, and using the methods outlined in this work, might also be sensitive to \mathcal{TM} . Searching for a $\mathcal{TM}\gamma$ final state from e^+e^- collisions has also been proposed [23], which may be accessible to Belle II. However, \mathcal{TM} discovery is not expected given the Belle II dark photon reach [24].

The rest of the paper is organized as follows. In Secs. II and III we describe the analogy between \mathcal{TM} and dark-photon and highlight the differences. Section IV contains the details of the proposed LHCb search. We conclude in

*xabier.cid.vidal@cern.ch

†philten@cern.ch

‡jonathan.plews@cern.ch

§bshuve@g.hmc.edu

||yotam.soreq@cern.ch

Published by the American Physical Society under the terms of the [Creative Commons Attribution 4.0 International license](https://creativecommons.org/licenses/by/4.0/). Further distribution of this work must maintain attribution to the author(s) and the published article's title, journal citation, and DOI. Funded by SCOAP³.

Sec. V. The Appendices contains technical details and a discussion about \mathcal{TM} and new physics.

II. TRUE MUONIUM SIGNAL AS A DARK PHOTON

Dark photons are massive spin-1 states that couple via a kinetic mixing ϵ to the standard model (SM) photon:

$$\mathcal{L} \supset \frac{\epsilon}{2} F_{\mu\nu} F'^{\mu\nu}, \quad (1)$$

where $F^{\mu\nu}$ and $F'^{\mu\nu}$ are the dark photon and SM photon field strengths, respectively. The phenomenology of \mathcal{TM} is similar to that of a dark photon, and the mass and kinetic mixing are predicted by QED at leading order:

$$m_{\mathcal{TM}} = 2m_\mu - B_E \approx 211 \text{ MeV}, \quad (2)$$

$$\epsilon_{\mathcal{TM}} = \alpha^2/2 \approx 2.66 \times 10^{-5}, \quad (3)$$

where $B_E \approx m_\mu \alpha^2/4 = 1.41 \text{ keV}$ is the \mathcal{TM} binding energy, estimated in the nonrelativistic limit. Our result is in agreement with Ref. [25], where the kinetic mixing of hidden sector onium states was calculated. We emphasize that the above analogy between \mathcal{TM} and the dark photon is valid only at energies close to the \mathcal{TM} mass, as relevant to our study.

As noted earlier, \mathcal{TM} decays through the same kinetic mixing to an e^+e^- final state with a branching fraction of $\text{BR}(\mathcal{TM} \rightarrow e^+e^-) \approx 98\%$, while the subdominant decay mode has $\text{BR}(\mathcal{TM} \rightarrow 3\gamma) \approx 1.7\%$. The \mathcal{TM} lifetime at leading order is

$$\tau_{\mathcal{TM}} \approx \frac{6}{\alpha^5 m_\mu} \approx 1.8 \times 10^{-12} \text{ sec}. \quad (4)$$

Because of the forward coverage of LHCb, light particles produced within LHCb acceptance typically have large boosts. Given the expected boost of \mathcal{TM} within LHCb and the relatively long proper lifetime of 0.53 mm, the decay of \mathcal{TM} into e^+e^- within LHCb will typically produce a resolvable displaced vertex. While searches for long-lived particles typically focus on new BSM states [26], \mathcal{TM} is an example of a SM long-lived particle that can be searched for at LHCb. Predictions of the mass and lifetime at higher order than those derived here are available [22,27]; however, it is unlikely that LHCb will be sensitive to these higher order corrections.

Since \mathcal{TM} and dark photon phenomenology are similar, excluding \mathcal{TM} dissociation detailed in Sec. III, projected dark photon reaches from future experiments can provide a rough guide to \mathcal{TM} sensitivity. In Fig. 1 the dark photon parameter space is plotted in dark photon mass (m) and kinetic mixing (ϵ) using DARKCAST [28], where \mathcal{TM} corresponds to a single point given by the ϵ and m of

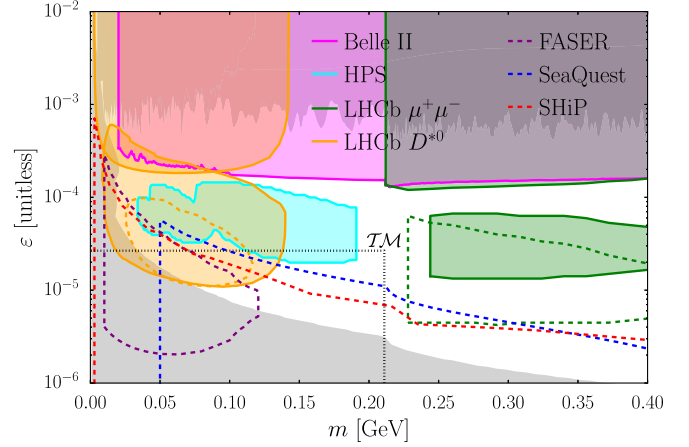


FIG. 1. Dark photon parameter space in dark photon mass and kinetic mixing with (gray) previous limits and future reach from (magenta) Belle II, (purple) FASER, (cyan) HPS, and (green/yellow) LHCb. \mathcal{TM} corresponds to the marked point, using Eqs. (2) and (3).

Eqs. (2) and (3). The gray regions correspond to already excluded parameter space, while the colored regions represent possible reach from relevant future experiments. Dashed lines indicate experiments where dissociation will be an issue. These include searches by FASER [29], SeaQuest [30], and SHiP [31] where \mathcal{TM} will dissociate as it passes through the shielding.

Both the proposed LHCb $D^{*0} \rightarrow D^0 A' (\rightarrow e^+e^-)$ [32] and inclusive $A' (\rightarrow \mu^+\mu^-)$ [33] searches are shown, to demonstrate how dark photon searches based on this study could be used to fill the gap between the two searches. The dashed regions for these LHCb searches correspond to post-module search strategies where the \mathcal{TM} will dissociate. The expected displaced reach of HPS [19] does not cover the \mathcal{TM} parameter space point, and will also suffer from some dissociation. Additionally, the expected prompt Belle II reach [24] does not extend to large enough lifetimes to discover \mathcal{TM} , and the nominal Belle II lifetime resolution will not be sufficient for effective displaced searches.

III. DISSOCIATION OF TRUE MUONIUM

Because \mathcal{TM} is a bound state rather than an elementary particle, there are significant differences between \mathcal{TM} and dark photon phenomenology. Most importantly, \mathcal{TM} can dissociate when the constituent muons of the bound state interact with the detector material, resulting in a separated μ^+ and μ^- with an invariant mass just above the mass of \mathcal{TM} , $m_{\mathcal{TM}}$.

The \mathcal{TM} dissociation cross section is estimated to be [34–37] $\sigma_{\mathcal{TM} \rightarrow \mu\mu} \approx 13Z^2 \text{b}$, where Z is the atomic number of the material inducing the dissociation. The bulk of the material traversed by \mathcal{TM} within LHCb prior to its decay is the aluminum radio frequency (rf)-foil (made of AlMg3) and the silicon vertex locator (VELO) sensors. Since both

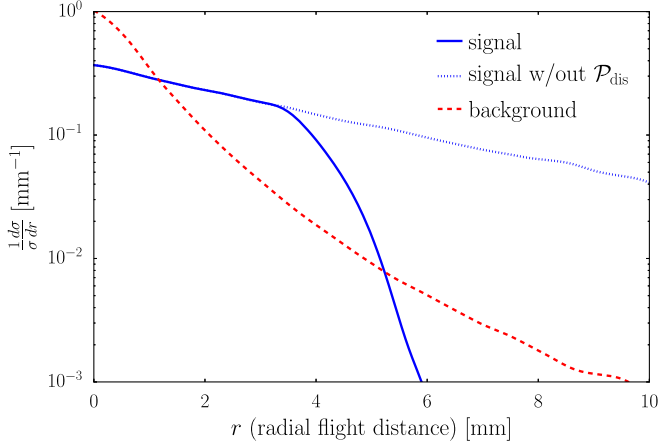


FIG. 2. Normalized radial flight distance distributions for the $\mathcal{TM} \rightarrow e^+e^-$ signal (blue solid) with dissociation, (blue dotted) without dissociation, and (red dashed) the e^+e^- background from B -hadron decays.

aluminum and silicon have similar Z and number densities, the mean free path for \mathcal{TM} traversing the material of the detector is,

$$\lambda^{-1} = \sigma_{\mathcal{TM} \rightarrow \mu\mu} n_a \approx 13 \text{ mm}^{-1}, \quad (5)$$

where the number density is $n_a \approx 6.0(5.0) \times 10^{19}$ atoms/mm³ [38] and $Z = 13(14)$ for aluminum (silicon). Thus, the probability of \mathcal{TM} dissociating is given by

$$\mathcal{P}_{\text{dis}} = 1 - e^{-x/\lambda}, \quad (6)$$

where x is the distance of the material traversed. The rf-foil will have a nominal width of 0.25 mm in Run 3 and the VELO sensors a nominal width of 0.2 mm. Consequently, every encounter of \mathcal{TM} with material in the VELO results in a minimum dissociation probability of $\mathcal{P}_{\text{dis}} \gtrsim 90\%$.

Given the expected material budget of the LHCb detector during Run 3 [5], the boost distribution for \mathcal{TM} produced within LHCb acceptance, and \mathcal{P}_{dis} , roughly half of the \mathcal{TM} produced are expected to dissociate without decaying into an e^+e^- final state. The radial flight distance distribution of the \mathcal{TM} particles which do decay into e^+e^- , is compared to the expected e^+e^- background in Fig. 2. On average, \mathcal{TM} has a higher boost than the background, resulting in a flatter distribution that is abruptly truncated by dissociation.

This dissociation gives rise to a signal of $\mu^+\mu^-$ originating from the regions of high material density at LHCb. While nearly half of the \mathcal{TM} produced is a considerable fraction of the total signal, the dissociated $\mu^+\mu^-$ signal is difficult to reconstruct and suffers from large irreducible backgrounds. The two muons will be nearly collinear and will typically share hits within the VELO, resulting in poorly defined tracks. Additionally, since the dissociation occurs in material, the conversion background of $\gamma \rightarrow \mu^+\mu^-$

can no longer be eliminated with a material veto without eliminating the signal itself. Therefore, for the remainder of the paper we focus on the 50% of signal events which decay via $\mathcal{TM} \rightarrow e^+e^-$.

IV. PROPOSED LHCb SEARCH

We propose searching for \mathcal{TM} as a displaced e^+e^- resonance. Since \mathcal{TM} behaves like a dark photon, the signal rate can be calculated directly from the off-shell photon rate as given by the prompt e^+e^- spectrum data [15,33,39]. For any initial (Y) and final (X) states, the ratio between the number of $Y \rightarrow X\mathcal{TM} \rightarrow Xe^+e^-$ events, $S_{\mathcal{TM}}$, and the number of prompt e^+e^- events, $Y \rightarrow X\gamma^* \rightarrow Xe^+e^-$, B_{EM} , is fixed. For the e^+e^- invariant mass within the range of $|m_{ee} - m_{\mathcal{TM}}| < 2\sigma_{m_{ee}}$, where $\sigma_{m_{ee}}$ is the e^+e^- invariant mass resolution, this ratio is given by

$$\frac{S_{\mathcal{TM}}}{B_{\text{EM}}} \approx \frac{3\pi m_\mu}{16\sigma_{m_{ee}}} \alpha^3 \approx \frac{20 \text{ MeV}}{\sigma_{m_{ee}}} 1.2 \times 10^{-6}. \quad (7)$$

The dominant source of off-shell photons in the mass range $m_{\mathcal{TM}} \approx 211$ MeV is from $\eta \rightarrow \gamma\gamma^*$ decays. We therefore focus on searching for \mathcal{TM} produced from $\eta \rightarrow \gamma\mathcal{TM}$ decays with a $\mathcal{TM} \rightarrow e^+e^-$ final state. The signal can be fully normalized by the data using the procedure outlined above. The ratio of Eq. (7) must be corrected by the different acceptance and efficiency factors for a displaced e^+e^- signal relative to the prompt signal. Additionally, the signal rate should be corrected by the expected dissociation factor, to account for \mathcal{TM} that dissociate without decaying.

The number of signal events can be estimated as follows: we simulate in PYTHIA 8.2 [40] both the pp total cross section, $\sigma_{\text{tot}} = 100$ mb, and the average number of η mesons produced per collision within the LHCb acceptance, $N_\eta = 0.83$. The former is in agreement with the LHCb inelastic cross section measurement [41], while the latter correctly predicts the low mass limit of the LHCb inclusive $\mu^+\mu^-$ dark photon search [39]. Given that $\text{BR}(\eta \rightarrow \gamma\mathcal{TM}) = 4.8 \times 10^{-10}$ [22], which agrees well with Eq. (7) using the differential $\eta \rightarrow \gamma e^+e^-$ shape from PYTHIA, the signal cross section in the fiducial volume is

$$\sigma_{\mathcal{TM}}^{\text{fid}} = \sigma_{\text{tot}} N_\eta \text{BR}(\eta \rightarrow \gamma\mathcal{TM}) \approx 40 \text{ pb}. \quad (8)$$

In our analysis we consider two possible search strategies: (i) inclusive search—the final state is e^+e^- and we do not search for the photon, thus the η is not reconstructed (in principle this search is sensitive to any \mathcal{TM} production mechanism); (ii) exclusive search—the final state is γe^+e^- and the η is reconstructed. Each of these methods has both advantages and disadvantages. The inclusive search is simpler and expected to have smaller systematic uncertainties, while the background rates for the exclusive analysis are smaller. Without a full detector simulation and data-driven

background estimates with their corresponding uncertainties, we cannot definitively state which of the two strategies is optimal; we therefore estimate the potential sensitivities of both. The details of our signal and background simulations are provided in Appendix A.

The LHCb experiment is a forward arm spectrometer which covers pseudorapidities between 2 and 5 [42,43]. This is a simplification of the coverage provided by the individual subsystems, but provides an adequate description, given the evolving nature of the upgraded detector and the weak assumptions made on electron identification efficiencies in this paper. While the exact performance of LHCb during Run 3 and 4 is yet to be fully understood, we estimate the relevant quantities as follows, with more details given in Appendix B. The e^+e^- invariant mass resolution around the \mathcal{TM} mass is estimated to be $\sigma_{m_{ee}} \approx 20$ MeV, based on the $K_S^0 \rightarrow e^+e^-e^+e^-$ LHCb study [44], while $\sigma_{m_{ee\gamma}}$ around the η mass is estimated to be 50 MeV based on Refs. [43,45,46].

We apply the following baseline selection criteria for both cases (i) and (ii):

- (1) Two opposite-sign electrons in the LHCb acceptance and with $p(e^\pm) > 10$ GeV, $p_T(e^\pm) > 0.5$ GeV, and transverse impact parameter (IP_T) which is not consistent with zero, $IP_T(e^\pm) > 3\sigma_{IP_T(e)}$, where $\sigma_{IP_T(e)}$ is the IP_T resolution;
- (2) A reconstructed $\mathcal{TM} \rightarrow e^+e^-$ candidate in the LHCb acceptance and with $p_T(\mathcal{TM}) > 1.0$ GeV, $|m_{ee} - m_{\mathcal{TM}}| < 2\sigma_{m_{ee}}$, and the distance of closest approach (DOCA) between the two electrons consistent with zero, $DOCA(e^+, e^-) < 3\sigma_{DOCA(e^+, e^-)}$ (the details on DOCA resolution are given in the Appendix B). This ensures that the electron pair forms a high-quality vertex.

For case (ii), in which we reconstruct the additional photon from the η decay, there are two additional baseline selections:

- (3) A photon in the LHCb acceptance and $p(\gamma) > 5$ GeV, and $p_T(\gamma) > 0.65$ GeV;
- (4) A reconstructed η candidate within the LHCb acceptance and $|m_{ee\gamma} - m_\eta| < 2\sigma_{m_{ee\gamma}}$.

For both cases (i) and (ii), data is expected to be collected using an e^+e^- trigger. During Run 1 and 2, only a single electron trigger with tight kinematic cuts was available in the first-level hardware trigger, which is not efficient for this signal. However, in Run 3 and 4 full online reconstruction with triggerless readout will be available [7], which will allow the reconstruction of lower momentum signals such as the electrons from \mathcal{TM} decays. Because \mathcal{TM} decays are displaced and inside a narrow invariant mass window, the \mathcal{TM} candidates can be reconstructed and recorded in Run 3 and 4 with a high efficiency.

The dominant background after the baseline selection is from B -hadron decays, which are also displaced. Decays of D -hadrons are a subdominant background since these rarely produce an e^+e^- pair which creates a reconstructible

vertex in the chosen kinematic regime. The background from photon conversions was also estimated and found to be subdominant, using techniques from the proposed $D^{*0} \rightarrow D^0 e^+e^-$ dark photon search [32] and a material veto similar to that used in the LHCb inclusive $\mu^+\mu^-$ dark photon search [47]. In the same regard, the background from $\eta \rightarrow e^+e^-\gamma$ decays will be also subdominant taking into account the expected displacement of the \mathcal{TM} before decaying (see Fig. 2). Given the excellent LHCb resolution for reconstructing the signal decay vertex [48], a moderate cut in this displacement would be enough to reduce this background to negligible levels.

B -mesons tend to decay to a high multiplicity of tracks that originate from the same decay vertex. These events are, in principle, readily suppressed by B -decay vetoes used in the LHCb dark photon search [39] and $B_s^0 \rightarrow \mu^+\mu^-$ lifetime measurement [49]. As a simple proxy for these vetoes, we apply the following additional selections:

- (i) The \mathcal{TM} candidate is isolated from other tracks in the LHCb acceptance: tracks with $p_T(\text{trk}) > 0.5$ GeV and $IP_T(\text{trk}) > 3\sigma_{IP_T(\text{trk})}$ must satisfy $DOCA(\text{trk}, e) > 3\sigma_{DOCA(\text{trk}, e)}$ for both electrons.
- (ii) The opening angle, θ , between the flight and momentum vectors of the \mathcal{TM} candidate is consistent with zero. The resolution on this opening angle depends upon the reconstructed flight distance and IP_T resolution of the two electrons.

The numbers of expected \mathcal{TM} candidates are given in Table I for the signal and background after the baseline selection, as well as after each of the two additional requirements. Less than 0.1% of the signal events pass the baseline selection, largely due to the inefficiency of the p_T requirements; however, the p_T selections cannot be significantly loosened. The efficiencies of the additional selections beyond baseline, however, are of order one for the signal and $\sim 10^{-3}$ – 10^{-4} for the background, allowing for efficient background reduction. There is an additional efficiency for reconstruction of all the final-state particles, ϵ_f , which originates from the reconstruction of the tracks, both online and offline, and from applying particle identification criteria. Because the expected electron and photon efficiencies are not yet public for Runs 3 and 4, we leave ϵ_f as an unspecified quantity in our expression for the

TABLE I. Expected signal and background yields for the $ee(ee\gamma)$ final state label as i (ii), assuming 100% reconstruction efficiency for the final state and a collected Run 3 dataset of 15 fb^{-1} .

requirement	$S_{\mathcal{TM}}^{(i)}$	$B_{\text{tot}}^{(i)}$	$S_{\mathcal{TM}}^{(ii)}$	$B_{\text{tot}}^{(ii)}$
base	3.4×10^3	3.2×10^7	1.6×10^3	5.4×10^6
DOCA(trk, e)	3.0×10^3	8.5×10^6	1.3×10^3	1.1×10^6
θ	1.5×10^3	1.8×10^4	6.4×10^2	1.9×10^3
efficiency	4.4×10^{-1}	5.6×10^{-4}	4.0×10^{-1}	3.5×10^{-4}

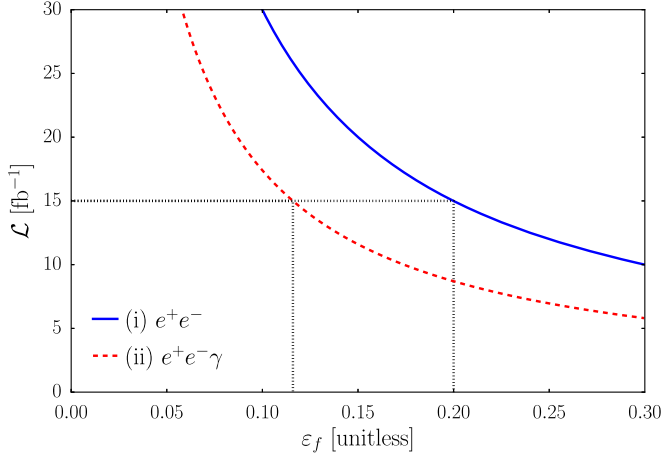


FIG. 3. The required integrated luminosity for a $5\sigma_{\text{stat}}$ discovery of $\mathcal{T}M$ as function of the final reconstruction efficiency, ϵ_f for the proposed (blue) e^+e^- and (red) $e^+e^-\gamma$ searches.

significance and discuss the implications shortly. We note that final state reconstruction efficiencies can be estimated based on current LHCb performance. From the $B \rightarrow J/\psi K^{*0}$ analysis [50] we find that $\epsilon_{e^+e^-} > 10\%$, and from Ref. [45] we estimate $\epsilon_{\gamma e^+e^-} \approx 0.3\epsilon_{e^+e^-} > 3\%$. For further details see Appendix B.

Because the background rate in the signal region can be estimated using the invariant mass sidebands, we expect the significance to be limited by the statistical uncertainty of the sample. The LHCb inclusive dark photon dimuon search [39] successfully used such a technique [51], although inclusion of known background structure helped improve significance. The shape of the B -hadron background

has been demonstrated to be well modeled [39], and there is a similar expectation for this analysis. Therefore, the $\mathcal{T}M$ signal significance is approximately given by

$$\sigma_{\text{stat}} \approx \frac{S_{\mathcal{T}M}}{\sqrt{B_{\text{tot}}}} \sqrt{\frac{\epsilon_f \mathcal{L}}{15 \text{ fb}^{-1}}}, \quad (9)$$

where $S_{\mathcal{T}M}$ and B_{tot} are the expected number of signal and background events from Table I, ϵ_f is the final state reconstruction efficiency, and \mathcal{L} is the integrated luminosity of the dataset. Using the expected Run 3 dataset of 15 fb^{-1} , $\mathcal{T}M$ can be discovered with $\sigma_{\text{stat}} \geq 5$ when $\epsilon_f > 20\%$ (12%) for the e^+e^- ($e^+e^-\gamma$) final state. Given the current LHCb performance, these efficiencies are realistic; see the above discussion and Appendix B. In Fig. 3 we plot the required integrated luminosity for discovery of $\mathcal{T}M$, e.g., $\sigma_{\text{stat}} \geq 5$, as a function of ϵ_f .

In addition, Fig. 4 shows the differential cross sections with respect to the e^+e^- invariant mass for signal and combinatorial background at LHCb, assuming a global efficiency to reconstruct the $\mathcal{T}M$ candidates of 20%, or 6% when also considering the reconstruction of the additional photon from the η decay.

We conclude this section by commenting that we considered additional selection criteria that we found to be sub-optimal and therefore did not include in our analysis. First, we can require that the IP_T of the two electrons, projected onto the normal of the decay plane, is consistent with zero. The decay plane is defined by the first hit of each electron track and the primary vertex. We found that this observable does not provide strong separation after the above selection has been applied. Second, the expected proper lifetime of the $\mathcal{T}M$ candidate is known, and so in principle the

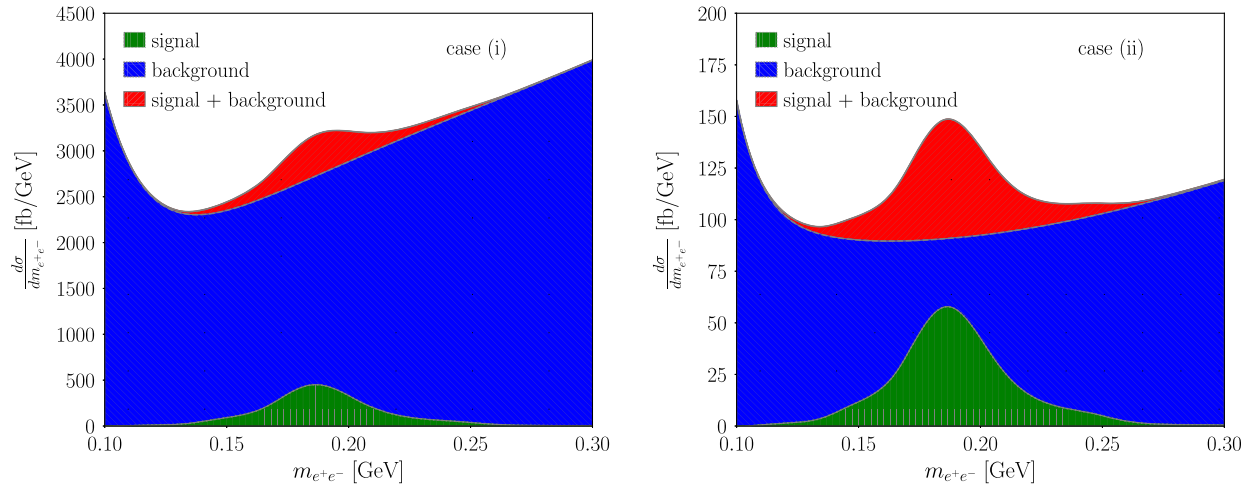


FIG. 4. The differential cross sections with respect to the e^+e^- invariant mass for the expected $\mathcal{T}M$ signal and combinatorial background at LHCb, assuming the normalization in Table I for case (i) and (ii). Global efficiencies of 20% and 6% are assumed to reconstruct the $\mathcal{T}M$ and $\mathcal{T}M$ plus photon candidates, respectively. In these conditions, a 5σ observation would be possible with an integrated luminosity of 15 fb^{-1} in case (i) and of 30 fb^{-1} in case (ii). The invariant mass resolution of the signal is described in the text. The shift observed in the central position of the signal peak, due to the lack of reconstructed bremsstrahlung from the electrons, is compatible with that of Ref. [44]. For the combinatorial background, the resulting invariant mass distribution is obtained from simulation.

transverse flight distance can be used to select events that are most consistent with this hypothesis. However, the analysis is more robust if no assumption is placed on the lifetime of the \mathcal{TM} candidate, and it does not appear to be necessary to reach a $5\sigma_{\text{stat}}$ discovery significance.

V. DISCUSSION AND OUTLOOK

As outlined above, we project that LHCb will be able to discover \mathcal{TM} with a statistical significance exceeding $5\sigma_{\text{stat}}$ in Run 3. Ultimately, LHCb and other experiments can directly measure the \mathcal{TM} mass, lifetime, and production rate (from η decays or other mechanisms). Since the \mathcal{TM} properties are well predicted by the SM, this will be a test of the SM predictions in Eqs. (2)–(4), and any deviation from them is a clear sign of new physics coupled to muons. Examples include dark photons, $L_\mu - L_\tau$ gauge bosons, scalars, or axionlike particles. In the presence of any of these particles, the \mathcal{TM} mass (via the binding energy), lifetime, branching ratios and spectroscopy (see discussion in [52]) are modified, and thus \mathcal{TM} measurements can discover or constrain new muonic interactions. Such new forces are motivated by several possible discrepancies with predictions of the SM in other experiments, including measurements of the muon anomalous magnetic moment $(g-2)_\mu$ [53], and the proton charge radius problem [54–57]. However, strong constraints on new physics exist from direct searches [58,59], measurements of $(g-2)_\mu$, neutrino experiments [60–66], and $e\mu$ spectroscopy [67–69]. Indeed, these constraints are generally more powerful than the expected sensitivity of LHCb to \mathcal{TM} , although some exceptions exist (for example, $(g-2)_\mu$ constraints can be alleviated if there are other new particles whose effects partially cancel). New muonic forces can also be probed as in Refs. [70–75]. For a detailed analysis see Appendix C.

In the context of this study, we also considered the possibility of an inclusive search for a $\tau^+\tau^-$ bound state, see e.g., Ref. [20]. In particular, orthotauonium, with a significant branching fraction to $\mu^+\mu^-$, would appear to be the best candidate for an LHCb search. We find, however, that the short lifetime of the tauonium (close to the τ itself), and the small signal yield compared to the background make the prospects very poor for being observed at LHCb.

In summary, we have studied the potential for LHCb to discover an as-yet-undiscovered long-lived particle in the SM: the $\mu^+\mu^-$ true muonium bound state. We have proposed a search for the vector 1^3S_1 true muonium state, \mathcal{TM} , which kinetically mixes with the photon and decays to e^+e^- . We have demonstrated that a search for $\eta \rightarrow \gamma\mathcal{TM}$, $\mathcal{TM} \rightarrow e^+e^-$ can exceed a $5\sigma_{\text{stat}}$ statistical significance using a displaced vertex search, and we have presented two possible searches: an inclusive search for the e^+e^- vertex, as well as an exclusive search where we reconstruct the additional photon and require $m(\gamma, \mathcal{TM}) = m_\eta$. Since \mathcal{TM} mixes kinetically with the photon and has a signature similar

to the dark photon, this method could also have sensitivity to dark photons in a similar mass window.

ACKNOWLEDGMENTS

We thank Gil Paz, Mike Williams and Jure Zupan for useful discussions, and Johannes Albrecht, Matthew John Charles, Maxim Pospelov, Mike Williams and José Zurita for comments on the manuscript. We also thank the organizers of the “New ideas in detecting long-lived particles at the LHC” workshop at LBL for a stimulating environment for discussions, along with other members of our working group: Jeff Asaf Dror, Maxim Pospelov, Yuhsin Tsai and José Zurita. The work of X. C. V. is supported by MINECO (Spain) through the Ramón y Cajal program RYC-2016-20073 and by XuntaGal under the ED431F 2018/01 project. P. I. is supported by a Birmingham Fellowship. J. P. is supported by the UK Science and Technology Facilities Council. The work of B. S. is supported by the U.S. National Science Foundation under Grant No. PHY-1820770.

APPENDIX A: SIGNAL AND BACKGROUND SIMULATION

All signal and background samples are simulated using PYTHIA 8.240 [40]. The signal from η meson decays is generated using the flag `SoftQCD:all = on`, while the B -hadron background is generated using the flag `HardQCD:bbbar = on`. For the latter, the `HardQCD` flag in conjunction with repeated B -hadron decays was used to generate a sufficiently large background sample. The results from this large sample were found to be in agreement with a smaller background sample generated using the more inclusive `SoftQCD` configuration. Additionally, including more sophisticated B -hadron decays using EVTGEN [76] was found to have no noticeable effect on the final result. This is because PYTHIA already uses the branching fraction tables from EVTGEN, and many of the inclusive EVTGEN decays use PYTHIA for showering and hadronization. The results from PYTHIA for both signal and background are demonstrated to be reliable, with the PYTHIA study of Ref. [33] accurately predicting the reach of the LHCb inclusive $\mu^+\mu^-$ dark photon search [39].

Conversion backgrounds were estimated using the photon flux generated from PYTHIA configured with the flag `SoftQCD:all = on`, and modeling the expected conversion rate within the material of the upgraded LHCb detector. The cross section for photon conversions was calculated using a method [77], similar to that implemented in the material simulation package GEANT [78]. The approximation of the opening angle between the converted electron-positron pair is underestimated at high masses by the GEANT model [79], and so a correction was applied to produce an invariant mass spectrum of the converted pair that matches the full analytic expression [80].

APPENDIX B: LHCb PERFORMANCE

1. Invariant mass resolution and reconstruction efficiencies

An upgraded version of the LHCb detector will record the result of proton-proton collisions at $\sqrt{s} = 14$ TeV during Runs 3 and 4 of the LHC. Similar, if not better, performances of the detector are expected during that period [4]. The upgrade of the detector is currently taking place. One important feature of this upgrade is the expected triggerless readout [7], removing the need for a first-level hardware trigger that is present in other LHC detectors. This will allow a dramatic increase in the efficiency to reconstruct low-momentum signatures, such as the decay products of $\mathcal{T}M$.

An estimation of the efficiency to reconstruct the $\mathcal{T}M$ candidates can be achieved by comparing to other LHCb analyses containing an e^+e^- final state. In the $B^0 \rightarrow J/\psi K^{*0}$ analysis, with the J/ψ decaying to an e^+e^- pair, reconstruction and selection efficiencies at the level of 5% could be achieved during the first years of LHCb running [50]. This efficiency includes the reconstruction of the accompanying K^{*0} particles decaying to $K\pi$ pairs as well as selection cuts on the mother B candidate. The kinematics of the selected $\mathcal{T}M$ signal electrons and those from J/ψ decay have been checked to be in reasonable agreement. Therefore, reconstruction and selection efficiencies above 10% should be easy to achieve. Since the performance of the upgraded LHCb detector is still to be determined, we chose to show the expected significance as a function of the final state reconstruction efficiency, rather than choosing a fixed value. This efficiency will also account for additional selection requirements to be applied in the experimental analysis. This includes the use of particle identification cuts or more sophisticated variables to discriminate against the combinatorial background. In the same regard, additional potential inefficiencies in the online reconstruction at the upgraded detector can be factorized as part of that efficiency. It should be remarked that the 5% efficiency, given as a baseline above, already includes this online reconstruction in the current detector.

One of the main challenges to reconstruct low momentum electrons at LHCb is the fact that the magnet sweeps away an important fraction of these particles, which then only leave hits in the pre-magnet tracking stations. Therefore, these electrons can be reconstructed, but their momenta are unknown. However, for the reconstruction of the $\mathcal{T}M$ mass, the knowledge of the pp collision vertex (where the $\mathcal{T}M$ was produced), the $\mathcal{T}M$ decay position, and the directions and momenta of the decay electrons is overconstrained. In this case, only the full reconstruction of one of the final-state electrons is necessary. For the other electron, only the direction is needed, such that hits in the pre-magnet tracking stations would be sufficient. The use of this technique could significantly increase the

reconstruction efficiency of the $\mathcal{T}M$ final state. One drawback of reconstructing electrons that are swept away by the magnet is the missing information from the PID detectors located after the magnet, e.g., RICH 2, the calorimeters, and the muon system. However, the PID information from RICH 1, specially designed for low-momentum particles [81], would still be available.

Concerning the e^+e^- invariant mass resolution for the $\mathcal{T}M$ reconstruction, Ref. [44] claims an invariant mass resolution of $\sim 8\%$ to reconstruct $K_S^0 \rightarrow e^+e^-e^+e^-$ decays at LHCb. The kinematic cuts in that study are softer with respect to this one, and therefore the momentum resolution for the electrons in this analysis is expected to be better, due to the smaller effect of multiple scattering. However, here we assume a similar invariant mass resolution, taking $\sigma_{m_{ee}} \sim 20$ MeV with radiative tails based on the invariant mass distribution from $K_S^0 \rightarrow e^+e^-e^+e^-$ decays. This conservative approach can be confirmed by the $\sigma_{m_{ee}}$ distribution from $B^0 \rightarrow J/\psi K^{*0}$ decays, with the J/ψ decaying to an e^+e^- pair [82]. For these decays, using final state electrons in a kinematic range similar to this study, resolutions at the level of 2% can be achieved with LHCb. The kinematic constraint mentioned above, arising from the knowledge of the $\mathcal{T}M$ decay position and the pp collision point, could also be used to improve the e^+e^- invariant mass resolution by $\approx 20\%$.

The full reconstruction of the $\eta \rightarrow \gamma\mathcal{T}M$ decay also requires the determination of the reconstruction efficiency of the γ . To obtain this, Ref. [45] is used, aligning our γ selection cuts with those in that analysis. In that study, an efficiency of 10% is claimed to reconstruct the photon. This includes both the effect of the kinematic cuts applied and of the reconstruction in the LHCb electromagnetic calorimeter (ECAL). If the effect of the kinematic cuts is factored out, an efficiency of $\approx 30\%$ is obtained. This is taken as a baseline for this analysis. In order to estimate the $\eta \rightarrow \gamma\mathcal{T}M$ decay invariant mass resolution, an estimate of the γ momentum resolution is needed. This has two components, the direction and energy resolution of the photons. The first depends on the ECAL cell size and on its distance to the pp collision point. Most of the signal photons are found to fall in the most inner region of the ECAL, where the cells have a size of ≈ 4 cm [43]. This provides an angular resolution of ≈ 0.002 . For the energy resolution, Ref. [43] reports $\delta E/E \approx 9\% \sqrt{\text{GeV}/E} \oplus 0.8\%$. Combining both effects together, an invariant mass resolution of $\sigma_{m_{e\gamma}} \approx 50$ MeV is obtained. The methodology is validated using multiple LHCb analyses with γ in the final states [45,46].

2. Impact parameter and DOCA resolution

The description of the upgraded LHCb vertex locator (VELO) is taken from Ref. [5], using a nominal single hit resolution of $12 \mu\text{m}$ in x and y . Multiple scattering is modeled [83] assuming an rf-foil thickness of 0.25 mm and

sensor thicknesses of 0.2 mm. This material description is validated against the full LHCb upgrade simulation where the transverse impact parameter for a track is parameterized by,

$$\sigma_{\text{IP}_T} = \left(1.1 + \frac{1.3 \text{ GeV}}{p_T} \right) \times 10^{-2} \text{ mm}, \quad (\text{B1})$$

where the first term is determined by the detector geometry and the second term arises from multiple scattering. The uncertainty on the distance of closest approach (DOCA) between two tracks is well approximated as,

$$\sigma_{\text{DOCA}} = \sigma_{\text{IP}_T}^{(1)} \oplus \sigma_{\text{IP}_T}^{(2)}, \quad (\text{B2})$$

given $\sigma_{\text{IP}_T}^{(1)}$ and $\sigma_{\text{IP}_T}^{(2)}$ are the IP_T uncertainties for the first and second track, respectively.

APPENDIX C: MUONIUM AND PHYSICS BEYOND THE STANDARD MODEL

Since the properties of \mathcal{TM} are completely determined by the SM, the ability of LHCb to independently measure the mass, production rate, and lifetime of \mathcal{TM} provides the possibility of a precision test of the SM. New particles and forces coupled to muons, including dark photons, $L_\mu - L_\tau$ gauge bosons, low-mass scalars, and axionlike particles, could potentially alter the muon binding energy and \mathcal{TM} decay rates by providing additional annihilation channels for the $\mu^+\mu^-$ bound state. Such new muonic forces have already been predicted in the context of the persistent anomalous measurements of $(g-2)_\mu$ and the proton charge radius problem, see e.g., [84].

Here, we focus on BSM contributions to the \mathcal{TM} decay rate, both to SM states mediated by new interactions but also the \mathcal{TM} decay to hidden-sector states. Since the \mathcal{TM} production rate depends on the \mathcal{TM} wave function at the origin, a new force can only appreciably modify this if its structure constant is comparable to α . However, this structure constant is strongly constrained by $(g-2)_\mu$ and other precision measurements. Therefore, the prospects for BSM modifications to the \mathcal{TM} decay are more promising than for its production, although still challenging to observe.

1. Hidden-sector models

We consider the following scenarios, which give rise to modifications of the \mathcal{TM} decay rate and branching fractions:

$$\text{Scalar } (S): \mathcal{L}_S = y_{S\mu} S \bar{\mu} \mu + y_{Se} S \bar{e} e, \quad (\text{C1})$$

$$\text{Pseudoscalar } (a): \mathcal{L}_a = y_{a\mu} a \bar{\mu} \gamma^5 \mu + y_{ae} a \bar{e} \gamma^5 e + \frac{g_{a\gamma}}{4} a F_{\mu\nu} \tilde{F}^{\mu\nu}, \quad (\text{C2})$$

$$\text{Vector } (V): \mathcal{L}_V = g_{V\mu} \bar{\mu} \gamma^\nu \mu V_\nu + g_{Ve} \bar{e} \gamma^\nu e V_\nu, \quad (\text{C3})$$

$$\text{Axial Vector } (A): \mathcal{L}_A = g_{A\mu} \bar{\mu} \gamma^\nu \gamma^5 \mu A_\nu + g_{Ae} \bar{e} \gamma^\nu \gamma^5 e A_\nu, \quad (\text{C4})$$

where $\tilde{F}^{\mu\nu} = \epsilon^{\mu\nu\rho\sigma} F_{\rho\sigma}/2$.

2. \mathcal{TM} decay to a photon and a mediator

If the mediator $X = S, a, V$ or A couples to muons, we can have decays as $\mathcal{TM} \rightarrow \gamma X$ or $\mathcal{TM} \rightarrow XX$. Since the decay to two mediators is typically suppressed by the square of the mediator coupling to muons, the decay to γX is the most important. Depending on the lifetime of X and its decay modes, the signature can be mono-photon, or photon and e^+e^- . Assuming that $\Gamma_{\mathcal{TM}} \approx \Gamma_{\mathcal{TM} \rightarrow e^+e^-}$, see Eq. (4), we find the following branching ratios

$$\text{BR}(\mathcal{TM} \rightarrow \gamma S) = \frac{y_{S\mu}^2}{2\pi\alpha(1-x_S)} (1 + 4x_S + x_S^2), \quad (\text{C5})$$

$$\text{BR}(\mathcal{TM} \rightarrow \gamma a) = \frac{(1-x_a)}{2\pi\alpha} \left[y_{a\mu}^2 + g_{a\gamma}^2 m_{\mathcal{TM}}^2 \frac{(1-x_a)^2}{16} \right], \quad (\text{C6})$$

$$\text{BR}(\mathcal{TM} \rightarrow \gamma V) = 0, \quad (\text{C7})$$

$$\text{BR}(\mathcal{TM} \rightarrow \gamma A) = \frac{g_{A\mu}^2}{2\pi\alpha} \frac{1 + 10x_A + x_A^2}{1-x_A}, \quad (\text{C8})$$

where $x_X = m_X^2/m_{\mathcal{TM}}^2$ and we neglect the relative momentum of the muons in the \mathcal{TM} state. This is reasonable because this kinetic energy is a small contribution to the energy released in the \mathcal{TM} decay.

The limits on the coupling of the mediator to muons is generally model dependent. However, the measurement of $(g-2)_\mu$ provides a sensitive probe of new physics coupled to muons. In principle, it is generally possible to evade these constraints by having another contribution to $(g-2)_\mu$ that almost cancels the one from the mediator. In Fig. 5 we plot the maximal \mathcal{TM} branching ratio to final states in Eqs. (C5)–(C8) which is allowed by measurements of $(g-2)_\mu$ at the 5σ level, i.e., $\Delta a_\mu = \frac{1}{2}(g-2)_\mu(\text{obs}) - \frac{1}{2}(g-2)_\mu(\text{SM}) \in [-1.1, 6.9] \times 10^{-9}$ [53]. We do not include the effects of the coupling $g_{a\gamma}$ on the branching fraction to pseudoscalars because of the powerful constraints on direct searches for axion-like particles from LEP data, which lead to a negligible contribution to the \mathcal{TM} branching fraction into pseudoscalars [85–87]; see also a recent recast of PrimEx data [88,89]. The expressions for NP contributions to Δa_μ are taken from [87,90,91]. As we can see the maximal branching ratios are typically below the 1% level

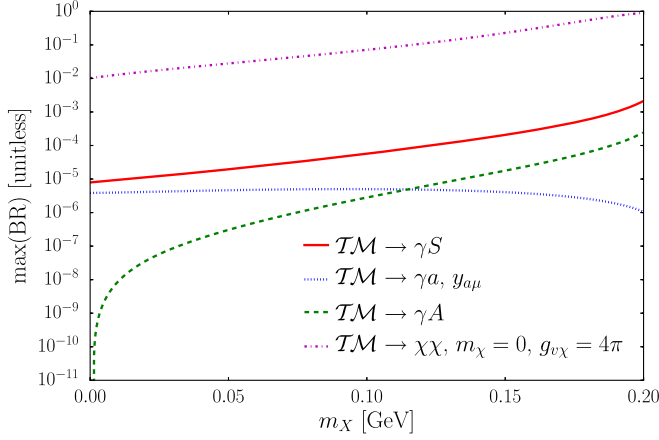


FIG. 5. \mathcal{TM} branching ratio to BSM final states in Eqs. (C5)–(C8) which are allowed by $(g-2)_\mu$ at the 5σ .

and require high precision \mathcal{TM} measurements to exceed this sensitivity.

3. \mathcal{TM} decay to hidden-sector particles

In this section, we calculate decay rates of \mathcal{TM} to hidden-sector particles χ such as $\mathcal{TM} \rightarrow \bar{\chi}\chi$, where χ is a hidden-sector particle. This results from muon annihilation via a s -channel mediator into the χ particles. This final state dominates when the mediator has a much larger coupling to hidden sector particles than SM particles. These χ particles could be invisible, or in turn decay to lighter hidden-sector particles. We consider the same mediators as in Sec. C 2 and assume that $m_{\mathcal{TM}} \neq m_\chi$; otherwise, we have to take into account mixing between the states. We note that the SM rate of $\mathcal{TM} \rightarrow Z^* \rightarrow \bar{\nu}\nu$ is completely negligible.

Let us assume for concreteness that χ is a Dirac fermion. The coupling to χ has the same parity structure as to SM leptons, e.g., we assume that a scalar couples to $\bar{\chi}\chi$, a pseudoscalar to $\bar{\chi}\gamma^5\chi$, etc. Because the \mathcal{TM} state we are considering is a vector, the only contribution is via decay through a vector state. Then, we have

$$\text{BR}(\mathcal{TM} \rightarrow V^* \rightarrow \bar{\chi}\chi) = \frac{g_{V\mu}^2 g_{V\chi}^2}{16\pi^2 \alpha^2 (1-x_V)^2} \times (1+2x_\chi) \sqrt{1-4x_\chi}. \quad (\text{C9})$$

If we consider $m_V < m_{\mathcal{TM}}$ such that there is no suppression of the V propagator and $m_\chi \ll m_{\mathcal{TM}}$, we obtain constraints on the coupling $g_{V\mu}$ from $(g-2)_\mu$. The coupling to ν_μ leads to constraints on neutrino trident rates, so for a vector coupling these also constrain $g_{V\mu}$. The maximal allowed value of $\text{BR}(\mathcal{TM} \rightarrow V^* \rightarrow \bar{\chi}\chi)$ by $(g-2)_\mu$ for $g_{V\chi} = 4\pi$ and $m_\chi = 0$ is plotted in Fig. 5. For $m_V \ll m_{\mathcal{TM}}$, this gives a hidden-sector branching fraction at the level of 2%. While this is likely too small to be seen as a change in the \mathcal{TM} lifetime or cross section, it could be detectable if the χ decays themselves are visible, which is challenging. If $m_V = 160$ MeV, the branching fraction is enhanced to $\sim 10\%$. If the states become much more degenerate than this, it is: (a) tuned; (b) would require some careful treatment of the width and mixing between the two states. This is especially true if the coupling $g_{V\chi}$ is very large, because the width would be large as well. If we instead take $g_{V\chi} = 1$, then the branching fraction is $\sim 10^{-4}$ for $m_V = 0$ and $\sim 10^{-3}$ for $m_V = 170$ MeV.

4. Modifications to \mathcal{TM} decay to e^+e^-

In this section, we consider s -channel contributions of the mediator to the decay of $\mathcal{TM} \rightarrow e^+e^-$. This is similar to the decay from Sec. C 3, but we must include interference with the contribution from the SM photon. We obtain (in the limit $m_e \ll m_{\mathcal{TM}}, m_V$)

$$\Gamma(\mathcal{TM} \rightarrow e^+e^-) = \frac{\alpha^3}{192\pi^2 (1-x_V)^2} \times [g_{V\mu} g_{Ve} + 4\pi\alpha(1-x_V)]^2, \quad (\text{C10})$$

which appropriately reduces to the V -only or photon-only results in the limits $\alpha \rightarrow 0$ and $g_{V\mu} = g_{Ve} = 0$, respectively. For $g_{V\mu}, g_{Ve} \ll \sqrt{4\pi\alpha}$, the dominant correction to the width from the SM value scales like

$$\frac{\Delta\Gamma}{\Gamma} = \frac{g_{V\mu} g_{Ve}}{2\pi\alpha(1-x_V)} \Big|_{x_V \ll 1} \lesssim 2 \times 10^{-5}. \quad (\text{C11})$$

Note that we can apply this to a dark photon by simply choosing $g_{Ve} = g_{V\mu} = \varepsilon\sqrt{4\pi\alpha}$, where ε is the kinetic mixing of the dark photon.

- [1] M. Deutsch, Evidence for the formation of positronium in gases, *Phys. Rev.* **82**, 455 (1951).
- [2] V. W. Hughes, D. W. McColm, K. Ziock, and R. Prepost, Formation of Muonium and Observation of its Larmor Precession, *Phys. Rev. Lett.* **5**, 63 (1960).
- [3] V. W. Hughes and B. Maglic, True muonium, *Bull. Am. Phys. Soc.* **16**, 65 (1971).
- [4] LHCb Collaboration, Framework TDR for the LHCb Upgrade: Technical design report, CERN Technical Report No. CERN-LHCC-2012-007/LHCb-TDR-12, 2012, <https://cds.cern.ch/record/1443882>.
- [5] LHCb Collaboration, LHCb VELO upgrade technical design report, CERN Technical Reports No. CERN-LHCC-2013-021, No. LHCb-TDR-013, 2013, <https://cds.cern.ch/record/1624070>.
- [6] LHCb Collaboration, LHCb PID upgrade technical design report, CERN Technical Report No. CERN-LHCC-2013-022/LHCb-TDR-014, 2013, <https://cds.cern.ch/record/1624074>.
- [7] LHCb Collaboration, LHCb trigger and online upgrade technical design report, CERN Technical Report No. CERN-LHCC-2014-016/LHCb-TDR-016, 2014, <https://cds.cern.ch/record/1701361>.
- [8] LHCb Collaboration, LHCb tracker upgrade technical design report, CERN Technical Report No. CERN-LHCC-2014-001/LHCb-TDR-015, 2014, <https://cds.cern.ch/record/1647400>.
- [9] R. Aaij *et al.* (LHCb Collaboration), Physics case for an LHCb Upgrade II—Opportunities in flavour physics, and beyond, in the HL-LHC era, [arXiv:1808.08865](https://arxiv.org/abs/1808.08865).
- [10] L. B. Okun, Limits of electrodynamics: Paraphotons?, *Zh. Eksp. Teor. Fiz.* **83**, 892 (1982) [*Sov. Phys. JETP* **56**, 502 (1982)].
- [11] P. Galison and A. Manohar, Two Z's or not Two Z's?, *Phys. Lett.* **136B**, 279 (1984).
- [12] B. Holdom, Two U(1)'s and Epsilon charge Shifts, *Phys. Lett.* **166B**, 196 (1986).
- [13] M. Pospelov, A. Ritz, and M. B. Voloshin, Secluded WIMP dark matter, *Phys. Lett. B* **662**, 53 (2008).
- [14] N. Arkani-Hamed, D. P. Finkbeiner, T. R. Slatyer, and N. Weiner, A theory of dark matter, *Phys. Rev. D* **79**, 015014 (2009).
- [15] J. D. Bjorken, R. Essig, P. Schuster, and N. Toro, New fixed-target experiments to search for dark gauge forces, *Phys. Rev. D* **80**, 075018 (2009).
- [16] J. Alexander *et al.*, Dark sectors 2016 Workshop: Community report, [arXiv:1608.08632](https://arxiv.org/abs/1608.08632).
- [17] J. Beacham *et al.*, Physics beyond colliders at CERN: Beyond the Standard Model working group report, [arXiv:1901.09966](https://arxiv.org/abs/1901.09966).
- [18] R. Essig *et al.*, Working group report: New light weakly coupled particles, in *Proceedings, 2013 Community Summer Study on the Future of U.S. Particle Physics: Snowmass on the Mississippi (CSS2013): Minneapolis, MN, USA* (2013).
- [19] N. Baltzell *et al.* (HPS Collaboration), The Heavy Photon Search beamline and its performance, *Nucl. Instrum. Methods Phys. Res., Sect. A* **859**, 69 (2017).
- [20] M. Fael and T. Mannel, On the decays $B \rightarrow K^{(*)} + \text{leptonium}$, *Nucl. Phys.* **B932**, 370 (2018).
- [21] C. Gatto, B. Fabela Enriquez, and M. I. Pedraza Morales (REDTOP Collaboration), The REDTOP project: Rare Eta decays with a TPC for optical photons, *Proc. Sci., ICHEP2016* (2017) 812.
- [22] Y. Ji and H. Lamm, Scouring meson decays for true muonium, *Phys. Rev. D* **99**, 033008 (2019).
- [23] S. J. Brodsky and R. F. Lebed, Production of the Smallest QED Atom: True Muonium ($\mu^+ \mu^-$), *Phys. Rev. Lett.* **102**, 213401 (2009).
- [24] W. Altmannshofer *et al.* (Belle-II Collaboration), The Belle II physics book, [arXiv:1808.10567](https://arxiv.org/abs/1808.10567).
- [25] H. An, B. Echenard, M. Pospelov, and Y. Zhang, Probing the Dark Sector with Dark Matter Bound States, *Phys. Rev. Lett.* **116**, 151801 (2016).
- [26] J. Alimena *et al.*, Searching for long-lived particles beyond the Standard Model at the Large Hadron Collider, [arXiv:1903.04497](https://arxiv.org/abs/1903.04497).
- [27] H. Lamm and Y. Ji, Predicting and discovering true Muonium ($\mu^+ \mu^-$), *EPJ Web Conf.* **181**, 01016 (2018).
- [28] P. Ilten, Y. Soreq, M. Williams, and W. Xue, Serendipity in dark photon searches, *J. High Energy Phys.* **06** (2018) 004.
- [29] A. Ariga *et al.* (FASER Collaboration), FASER's physics reach for long-lived particles, *Phys. Rev. D* **99**, 095011 (2019).
- [30] S. Gardner, R. J. Holt, and A. S. Tadepalli, New prospects in fixed target searches for dark forces with the SeaQuest experiment at Fermilab, *Phys. Rev. D* **93**, 115015 (2016).
- [31] S. Alekhin *et al.*, A facility to search for hidden particles at the CERN SPS: The SHiP physics case, *Rep. Prog. Phys.* **79**, 124201 (2016).
- [32] P. Ilten, J. Thaler, M. Williams, and W. Xue, Dark photons from charm mesons at LHCb, *Phys. Rev. D* **92**, 115017 (2015).
- [33] P. Ilten, Y. Soreq, J. Thaler, M. Williams, and W. Xue, Proposed Inclusive Dark Photon Search at LHCb, *Phys. Rev. Lett.* **116**, 251803 (2016).
- [34] S. Mrowczynski, Interaction of elementary atoms with matter. *Phys. Rev. A* **33**, 1549 (1986).
- [35] E. Holvik and H. A. Olsen, Creation of relativistic Fermionium in collisions of electrons with atoms, *Phys. Rev. D* **35**, 2124 (1987).
- [36] S. Mrowczynski, Interaction of relativistic elementary atoms with matter. 1. General formulas, *Phys. Rev. D* **36**, 1520 (1987).
- [37] K. G. Denisenko and S. Mrowczynski, Interaction of relativistic elementary atoms with matter. 2. Numerical results, *Phys. Rev. D* **36**, 1529 (1987).
- [38] M. Tanabashi *et al.* (Particle Data Group), Review of particle physics. *Phys. Rev. D* **98**, 030001 (2018).
- [39] R. Aaij *et al.* (LHCb Collaboration), Search for Dark Photons Produced in 13 TeV pp Collisions, *Phys. Rev. Lett.* **120**, 061801 (2018).
- [40] T. Sjöstrand, S. Ask, J. R. Christiansen, R. Corke, N. Desai, P. Ilten, S. Mrenna, S. Prestel, C. O. Rasmussen, and P. Z. Skands, An introduction to PYTHIA 8.2, *Comput. Phys. Commun.* **191**, 159 (2015).
- [41] R. Aaij *et al.* (LHCb Collaboration), Measurement of the inelastic pp cross-section at a centre-of-mass energy of 13 TeV, *J. High Energy Phys.* **06** (2018) 100.

- [42] A. A. Alves, Jr. *et al.* (LHCb Collaboration), The LHCb detector at the LHC, *J. Instrum.* **3**, S08005 (2008).
- [43] R. Aaij *et al.* (LHCb Collaboration), LHCb detector performance, *Int. J. Mod. Phys. A* **30**, 1530022 (2015).
- [44] C. Marin Benito, L. Garrido Beltran, and X. Cid Vidal, Feasibility study of $K_S^0 \rightarrow \pi^+\pi^-e^+e^-$ at LHCb, CERN Technical Reports No. LHCb-PUB-2016-016 and No. CERN-LHCb-PUB-2016-016, 2016, <https://cds.cern.ch/record/2193358>.
- [45] R. Aaij *et al.* (LHCb Collaboration), Measurement of the ratio of prompt χ_c to J/ψ production in pp collisions at $\sqrt{s} = 7$ TeV, *Phys. Lett. B* **718**, 431 (2012).
- [46] R. Aaij *et al.* (LHCb Collaboration), First Experimental Study of Photon Polarization in Radiative B_s^0 Decays, *Phys. Rev. Lett.* **118**, 021801 (2017); *Publisher's Note* **118**, 109901(A) (2017).
- [47] M. Alexander *et al.*, Mapping the material in the LHCb vertex locator using secondary hadronic interactions, *J. Instrum.* **13**, P06008 (2018).
- [48] R. Aaij *et al.*, Performance of the LHCb Vertex Locator, *J. Instrum.* **9**, P09007 (2014).
- [49] R. Aaij *et al.* (LHCb Collaboration), Measurement of the $B_s^0 \rightarrow \mu^+\mu^-$ Branching Fraction and Effective Lifetime and Search for $B^0 \rightarrow \mu^+\mu^-$ Decays, *Phys. Rev. Lett.* **118**, 191801 (2017).
- [50] M. Nicol, Analysis of the rare decay $B^0 \rightarrow K^{*0}e^+e^-$ at LHCb, Ph.D. thesis, Orsay, LAL, 2012, <http://tel.archives-ouvertes.fr/tel-00788992>.
- [51] M. Williams, A novel approach to the bias-variance problem in bump hunting, *J. Instrum.* **12**, P09034 (2017).
- [52] J. Jaeckel and S. Roy, Spectroscopy as a test of Coulomb's law: A probe of the hidden sector, *Phys. Rev. D* **82**, 125020 (2010).
- [53] G. W. Bennett *et al.* (Muon g-2 Collaboration), Final report of the Muon E821 anomalous magnetic moment measurement at BNL, *Phys. Rev. D* **73**, 072003 (2006).
- [54] P. J. Mohr, D. B. Newell, and B. N. Taylor, CODATA recommended values of the fundamental physical constants: 2014, *Rev. Mod. Phys.* **88**, 035009 (2016).
- [55] A. Beyer, L. Maisenbacher, A. Matveev, R. Pohl, K. Khabarova, A. Grinin, T. Lamour, D. C. Yost, T. W. Hänsch, N. Kolachevsky, and T. Udem, The rydberg constant and proton size from atomic hydrogen, *Science* **358**, 79 (2017).
- [56] C. E. Carlson, The proton radius puzzle, *Prog. Part. Nucl. Phys.* **82**, 59 (2015).
- [57] Z. Epstein, G. Paz, and J. Roy, Model independent extraction of the proton magnetic radius from electron scattering, *Phys. Rev. D* **90**, 074027 (2014).
- [58] J. P. Lees *et al.* (BABAR Collaboration), Search for a muonic dark force at BABAR, *Phys. Rev. D* **94**, 011102 (2016).
- [59] A. M. Sirunyan *et al.* (CMS Collaboration), Search for an $L_\mu - L_\tau$ gauge boson using $Z \rightarrow 4\mu$ events in proton-proton collisions at $\sqrt{s} = 13$ TeV, *Phys. Lett. B* **792**, 345 (2019).
- [60] S. R. Mishra *et al.* (CCFR Collaboration), Neutrino Tridents and W Z Interference, *Phys. Rev. Lett.* **66**, 3117 (1991).
- [61] G. Bellini *et al.*, Precision Measurement of the ^7Be Solar Neutrino Interaction Rate in Borexino, *Phys. Rev. Lett.* **107**, 141302 (2011).
- [62] R. Harnik, J. Kopp, and P. A. N. Machado, Exploring nu signals in dark matter detectors, *J. Cosmol. Astropart. Phys.* **07** (2012) 026.
- [63] M. Agostini *et al.* (Borexino Collaboration), First simultaneous precision spectroscopy of pp , ^7Be , and pep solar neutrinos with Borexino phase-II, [arXiv:1707.09279](https://arxiv.org/abs/1707.09279).
- [64] W. Altmannshofer, S. Gori, M. Pospelov, and I. Yavin, Neutrino Trident Production: A Powerful Probe of New Physics with Neutrino Beams, *Phys. Rev. Lett.* **113**, 091801 (2014).
- [65] G. Magill and R. Plestid, Neutrino trident production at the intensity frontier, *Phys. Rev. D* **95**, 073004 (2017).
- [66] W. Altmannshofer, S. Gori, J. Martín-Albo, A. Sousa, and M. Wallbank, Neutrino Tridents at DUNE, [arXiv:1902.06765](https://arxiv.org/abs/1902.06765).
- [67] S. G. Karshenboim, Precision Physics of Simple Atoms and Constraints on a Light Boson with Ultraweak Coupling, *Phys. Rev. Lett.* **104**, 220406 (2010).
- [68] S. G. Karshenboim, D. McKeen, and M. Pospelov, Constraints on muon-specific dark forces, *Phys. Rev. D* **90**, 073004 (2014); *Publisher's Note* **90**, 079905(A) (2014).
- [69] C. Fruguele, J. Pérez-Ríos, and C. Peset, Current and future perspectives of positronium and muonium spectroscopy as dark sectors probe, *Phys. Rev. D* **100**, 015010 (2019).
- [70] S. N. Gninenko, N. V. Krasnikov, and V. A. Matveev, Muon g-2 and searches for a new leptophobic sub-GeV dark boson in a missing-energy experiment at CERN, *Phys. Rev. D* **91**, 095015 (2015).
- [71] J. Grange *et al.* (Muon g-2 Collaboration), Muon (g-2) technical design report, [arXiv:1501.06858](https://arxiv.org/abs/1501.06858).
- [72] C.-Y. Chen, M. Pospelov, and Y.-M. Zhong, Muon beam experiments to probe the dark sector, *Phys. Rev. D* **95**, 115005 (2017).
- [73] M. Abe *et al.*, A new approach for measuring the Muon anomalous magnetic moment and electric dipole moment, *Prog. Theor. Exp. Phys.* **2019**, 053C02 (2019).
- [74] Y. Kahn, G. Krnjaic, N. Tran, and A. Whitbeck, M^3 : A new muon missing momentum experiment to probe $(g-2)_\mu$ and dark matter at Fermilab, *J. High Energy Phys.* **09** (2018) 153.
- [75] G. Krnjaic, G. Marques-Tavares, D. Redigolo, and K. Tobioka, Probing muonic forces and dark matter at Kaon factories, [arXiv:1902.07715](https://arxiv.org/abs/1902.07715).
- [76] D. J. Lange, The EvtGen particle decay simulation package, *Nucl. Instrum. Methods Phys. Res., Sect. A* **462**, 152 (2001).
- [77] H. Davies, H. A. Bethe, and L. C. Maximon, Theory of bremsstrahlung and pair production. 2. Integral cross section for pair production, *Phys. Rev.* **93**, 788 (1954).
- [78] S. Agostinelli *et al.* (GEANT4 Collaboration), GEANT4: A simulation toolkit, *Nucl. Instrum. Methods Phys. Res., Sect. A* **506**, 250 (2003).
- [79] R. Brun, F. Bruyant, F. Carminati, S. Giani, M. Maire, A. McPherson, G. Patrick, and L. Urban, GEANT detector description and simulation tool.
- [80] Y.-S. Tsai, Pair production and bremsstrahlung of charged leptons, *Rev. Mod. Phys.* **46**, 815 (1974); *Erratum* **49**, 421 (1977).
- [81] M. Adinolfi *et al.* (LHCb RICH Collaboration), Performance of the LHCb RICH detector at the LHC, *Eur. Phys. J. C* **73**, 2431 (2013).

- [82] R. Aaij *et al.* (LHCb Collaboration), Test of lepton universality with $B^0 \rightarrow K^{*0} \ell^+ \ell^-$ decays, *J. High Energy Phys.* **08** (2017) 055.
- [83] G. R. Lynch and O. I. Dahl, Approximations to multiple Coulomb scattering, *Nucl. Instrum. Methods Phys. Res., Sect. B* **58**, 6 (1991).
- [84] D. Tucker-Smith and I. Yavin, Muonic hydrogen and MeV forces, *Phys. Rev. D* **83**, 101702 (2011).
- [85] S. Knapen, T. Lin, H. K. Lou, and T. Melia, Searching for Axionlike Particles with Ultraperipheral Heavy-Ion Collisions, *Phys. Rev. Lett.* **118**, 171801 (2017).
- [86] J. Jaeckel and M. Spannowsky, Probing MeV to 90 GeV axion-like particles with LEP and LHC, *Phys. Lett. B* **753**, 482 (2016).
- [87] Y. Kahn, G. Krnjaic, S. Mishra-Sharma, and T. M. P. Tait, Light weakly coupled axial forces: Models, constraints, and projections, *J. High Energy Phys.* **05** (2017) 002.
- [88] I. Larin *et al.* (PrimEx Collaboration), A New Measurement of the π^0 Radiative Decay Width, *Phys. Rev. Lett.* **106**, 162303 (2011).
- [89] D. Aloni, C. Fanelli, Y. Soreq, and M. Williams, Photo-production of axion-like particles, [arXiv:1903.03586](https://arxiv.org/abs/1903.03586) [Phys. Rev. Lett. (to be published)].
- [90] B. Batell, N. Lange, D. McKeen, M. Pospelov, and A. Ritz, Muon anomalous magnetic moment through the leptonic Higgs portal, *Phys. Rev. D* **95**, 075003 (2017).
- [91] C.-Y. Chen, H. Davoudiasl, W. J. Marciano, and C. Zhang, Implications of a light dark Higgs solution to the $(g_\mu - 2)$ discrepancy, *Phys. Rev. D* **93**, 035006 (2016).